



# Enhanced photocatalytic activity of transition metal ions doped g-C<sub>3</sub>N<sub>4</sub> nanosheet activated by PMS for organic pollutant degradation

Arulappan Durairaj<sup>1</sup> · Thangavel Sakthivel<sup>2</sup> · Asir Obadiah<sup>1</sup> · Samuel Vasanthkumar<sup>1</sup>

Received: 27 November 2017 / Accepted: 27 February 2018 / Published online: 2 March 2018  
© Springer Science+Business Media, LLC, part of Springer Nature 2018

## Abstract

A layer nanostructure of g-C<sub>3</sub>N<sub>4</sub> catalyst doped with transition metals like Ni, Co, and Fe were synthesized. The structure morphology of the metal doped g-C<sub>3</sub>N<sub>4</sub> were studied using XRD, SEM-EDAX, UV-DRS and FT-IR spectroscopy techniques. The presence of transition metals enhanced the visible light absorbance and reduced the electron hole recombination. The efficiency of the catalyst was also enhanced using PMS activation and minimization of charge carrier recombination. The photocatalytic effect of the transition metal doped g-C<sub>3</sub>N<sub>4</sub> nanosheet activated by PMS on the degradation of organic pollutants like Reactive Red 120, Orange G and 2-Amino-4-chlorophenol was investigated. Degradation efficiency in the case of RR120 was nearly 100% with Co-C<sub>3</sub>N<sub>4</sub>-PMS-Light system in a time duration of 120 min. Whereas it was 60% in 2-amino-4-chlorophenol and 100% in orange-G, in the same catalyst system and time duration. The findings reveal that the catalyst could play a key role in the treatment of organic pollutants.

## 1 Introduction

Hazardous organic compounds are either used as reagents or formed as by products in many industries process. This ingestion of untreated perilous compounds can have been varying detrimental effects on the human body such as lethal effects like genotoxicity, mutagenicity and carcinogenicity [1]. Presently, available treatment of precarious compounds is expensive and the industry requires cost effective novel methods for treatment of such compounds. Photocatalytic is a zero waste techniques to treat the environmental hazardous in pioneering work TiO<sub>2</sub> was used as a catalyst, however there are several problems affecting the final efficiencies. To overcome the issues, discovery of new materials is an important at this moment. Two dimensional nanostructures have

a wide range of usage in the field of semiconductor photocatalysis for environmental and energy application research [2–4]. Some of the nanostructural two dimensional materials studied for photocatalysis applications are graphene, graphene oxide, graphdiyne and metal chalcogenides [5–7]. Many studies have been carried out on the morphology and structure dependent catalytic property of these nanostructured materials [8, 9]. In addition, doping and hybrid graphene structures have been shown to have better photocatalytic properties [10]. However, graphene compounds don't have a defined band gap, and therefore, they are not used as a standalone photocatalyst [11].

g-C<sub>3</sub>N<sub>4</sub> is layered semiconductor material with band gap energy of 2.5 eV [12]. The preparation of g-C<sub>3</sub>N<sub>4</sub> is simple, cost effective. Various precursor materials have been used to synthesis g-C<sub>3</sub>N<sub>4</sub> like dicyandiamide, urea and melamine [13–15]. Among the diverse synthesis methods, using urea as a precursor is very easy for preparing porous g-C<sub>3</sub>N<sub>4</sub> [16]. Recent studies have employed g-C<sub>3</sub>N<sub>4</sub> photocatalyst for H<sub>2</sub> production and organic pollutant degradation [17, 18]. The disadvantage of using g-C<sub>3</sub>N<sub>4</sub> is low reactivity towards a redox based reactions and its tendency for rapid charge carrier recombination. These disadvantages have been overcome by doping g-C<sub>3</sub>N<sub>4</sub> with metals [19]. Activation of the photocatalyst with PMS has also been investigated in a previous study [20].

**Electronic supplementary material** The online version of this article (<https://doi.org/10.1007/s10854-018-8826-5>) contains supplementary material, which is available to authorized users.

✉ Samuel Vasanthkumar  
kumar2359@yahoo.com

- <sup>1</sup> Department of chemistry, Karunya University, Karunya Nagar, Coimbatore, Tamil Nadu 641-114, India
- <sup>2</sup> Key Lab of Advanced Transducers and Intelligent Control System, Ministry of Education and Shanxi Province, College of Physics and Optoelectronics, Taiyuan University of Technology, Taiyuan 030024, People's Republic of China

Advanced oxidation technology like the catalytic ozone oxidation, Fenton and photocatalysis have been employed to degrade various pollutants [21, 22]. These technologies are energy efficient and eco-friendly and therefore have gained prominence. Because, sulfate radicals generated by PMS decomposition have outperformed the hydroxyl radicals. The sulfate free radical has a high reactive potential 2.5–3.1, a wide range of pH 2–9 and longer life time [23]. Peroxymonosulfate or Oxone is widely used for  $\text{SO}_4^{-2}$  radical generation using either homogenous or heterogeneous catalyst [24]. It is also known that PMS can be easily activated using heat, metal ions and UV irradiation [20, 25, 26]. C=O functional group strongly generated sulfate radicals via PMS decomposition [27]. Use of transition metal ions in PMS activation has some practical challenges such as reusing the catalyst and metal leaching property during the reaction [28]. To avoid this metal leaching during the reaction metal ions should be bind with supporting materials.

In this scenario  $g\text{-C}_3\text{N}_4$  is a promising material to binding the metal ions, since it contains a lone pair of electrons. Previously, metal doped  $g\text{-C}_3\text{N}_4$  was synthesized by in situ approach. However, this method contains few drawbacks like low packing of  $g\text{-C}_3\text{N}_4$  structure. In this work we prepared transition metal ions doped  $g\text{-C}_3\text{N}_4$  like  $\text{Co-C}_3\text{N}_4$ ,  $\text{Ni-C}_3\text{N}_4$ , and  $\text{Fe-C}_3\text{N}_4$  employing by a cost effective sonochemical approach. The prepared catalysts were studied for the degradation of organic pollutants like RR120, Orange G, and phenol derivative 2-Amino-4-chlorophenol. The PMS activation of the catalyst was investigated in the presence and absence of visible light. The electron hole recombination process was studied by PL spectra and the free radical was analyzed under controlled conditions using EtOH, t-BuOH scavengers.

## 2 Experiment

### 2.1 Materials

Urea ( $\text{CH}_4\text{N}_2\text{O}$ ), cobalt chloride hexahydrate ( $\text{CoCl}_2 \cdot 6\text{H}_2\text{O}$ ), iron sulfate ( $\text{FeSO}_4 \cdot x\text{H}_2\text{O}$ ) and nickel chloride ( $\text{NiCl}_2 \cdot 6\text{H}_2\text{O}$ ) were purchased from Sigma-Aldrich India. The organic compounds like Reactive red 120 ( $\text{C}_{44}\text{H}_{24}\text{C}_{12}\text{N}_{14}\text{O}_{20}\text{S}_8\text{Na}_8$ ), Orange G ( $\text{C}_{16}\text{H}_{10}\text{N}_2\text{Na}_2\text{O}_7\text{S}_2$ ), and chemical compound 2-Amino-4-chlorophenol ( $\text{C}_6\text{H}_6\text{ONCl}$ ) were purchased from Merck chemicals Ltd India. EtOH, t-BuOH and peroxymonosulfate ( $2\text{KHSO}_5 \cdot \text{KHSO}_4 \cdot \text{K}_2\text{SO}_4$ ) were purchased from Merck chemicals Ltd India. Double distilled water was used entire experiment.

### 2.2 Preparation of pure and metal doped $\text{C}_3\text{N}_4$

The preparation of pure and metal doped  $g\text{-C}_3\text{N}_4$  involves several stages. Urea is subjected to pyrolysis in a sealed crucible at  $450^\circ\text{C}$  for 2 h [14]. The sample is then allowed to cool to room temperature. The product obtained at the end of pyrolysis is porous  $g\text{-C}_3\text{N}_4$  (pale yellow color). The  $g\text{-C}_3\text{N}_4$  is then kept under ultrasonic irradiation in an ethanol medium for 30 min when the exfoliation occurs. The obtained exfoliated  $g\text{-C}_3\text{N}_4$  are effective catalysts for degradation of organic compounds, but they have a tendency towards charge carrier recombination [29]. To overcome this tendency, the pure  $g\text{-C}_3\text{N}_4$  is doped with various transition metal ions (Fe, Co, Ni) by the sonochemical method. The doped  $g\text{-C}_3\text{N}_4$  is again sonicated for 30 min. The particles are allowed to settle and the filtrate is discarded. The metal doped  $g\text{-C}_3\text{N}_4$  obtained is washed with a copious amount of ethanol and distilled water. During washing loosely bonded trace amount of the metal is removed. The reproducibility of the composite photocatalysts were examined and found to be good, and the materials are stable. Structural analysis carried out on the samples confirmed the stability and reproducibility of the materials.

### 2.3 Instrumentation

In this present study structure morphology, d-spacing, band gap, functional group, particle size, zeta potential and free radical production of the pure and metal doped  $g\text{-C}_3\text{N}_4$  was analyzed. The X-ray diffraction (XRD) patterns of metal hybrid  $\text{C}_3\text{N}_4$  were analyzed using an X-ray diffractometer (Shimadzu model: XRD 6000 with Cu  $\text{K}\alpha$  radiation) in the range of  $10^\circ\text{--}80^\circ$  and with a scanning speed of 10 deg/min. To study the morphology of the pure  $\text{C}_3\text{N}_4$  and the doped  $\text{C}_3\text{N}_4$  ( $\text{Co-C}_3\text{N}_4$ ,  $\text{Ni-C}_3\text{N}_4$  and  $\text{Fe-C}_3\text{N}_4$ ), a scanning electron microscope with equipped with EDAX (Model: JOEL JSM-6390 Hitachi S-4500) was used. The identification of the functional group was carried out using a Fourier transform infrared spectroscopy (Model: Nicolet-6700, USA) instrument. The Band gap and absorption behaviors of the  $\text{C}_3\text{N}_4$  and metal doped  $\text{C}_3\text{N}_4$  were analyzed using a DRS UV (Model: Shimadzu model) instrument. The behavior of photo emission, photoexcited charge carriers and recombination were analyzed using a photoluminescence spectrophotometer (Model: FLUOROLOG, HORIBAYVON). UV absorption spectra of photocatalyzed RR120, Orange G and 2-Amino-4-chlorophenol at different time intervals were recorded using a spectrophotometer (Model: JASCO V-670) at room temperature. Free radical analysis was carried out using classical quenching agent such as EtOH and t-BuOH.

## 2.4 Photocatalytic study and analysis

The photocatalytic degradation analysis of organic pollutants like RR120, Orange G and 2-amino-4-chlorophenol were studied using the pure and metal doped (Co, Ni and Fe)  $g\text{-C}_3\text{N}_4$ . The photocatalytic degradation process was carried out in a photocatalytic chamber under visible light condition at 380 nm using 6 W lamp. The metal doped and or pure  $g\text{-C}_3\text{N}_4$  was dispersed in double distilled water and this dispersed material was sonicated for 10 min. The organic pollutants were prepared in solutions of  $1 \times 10^{-5}$  M concentration. This solution amalgamation was mixed with catalyst and blends were then used for the photocatalytic study. The solution mixture was stirred for 30 min under dark condition to reach the adsorption de-adsorption equilibrium. The solution of photocatalyst and organic pollutant exposed to visible light to initiate photocatalysis. The absorbance spectra of the concentrate was followed a using UV-spectrometer every 30 min. Prior to recording of the absorbance spectra, a small sample from the mixture (3 ml) is centrifuged for 5 min to remove the catalyst. The effectiveness of the catalyst is evaluated using the formula given below.

$$\text{Degradation efficiency (DE\%)} = \left[ 1 - \frac{C_t}{C_0} \right] \times 100 \quad (1)$$

$$\ln \frac{C_t}{C_0} = -kt \quad (2)$$

Here  $C_0$  and  $C_t$  refer to the initial and time dependent concentration of the target molecule respectively. 't' refers to the reaction time and 'k' is the pseudo first order rate constant [30, 31]. Further analysis of the catalyst was based on scavenger study to determine the free radical behavior. Two different radical scavenger or quenching agents such as EtOH and t-BuOH were used with a different ratio. To examine

the reproducibility of the catalyst, four conservative cycle catalytic degradation was studied.

## 3 Results and discussion

The crystalline and phase properties of pure  $g\text{-C}_3\text{N}_4$  and metal doped  $g\text{-C}_3\text{N}_4$  were studied using the XRD method. Figure 1 represents the XRD spectra of pure  $g\text{-C}_3\text{N}_4$ , Co- $g\text{-C}_3\text{N}_4$ , Ni- $g\text{-C}_3\text{N}_4$ , and Fe- $g\text{-C}_3\text{N}_4$  nano structure. Pure  $g\text{-C}_3\text{N}_4$  shows a strong peak at  $27.88^\circ$  and shoulder peak at  $10.59^\circ$  which can be indexed as (111) and (100) plane. The calibration related to previous studies with similar d-spacing values of 3.1 and 8.3 nm respectively [32]. The calibration pertaining to metal doped  $g\text{-C}_3\text{N}_4$  shows a single strong peak at  $27.4^\circ$  where as the shoulder peak was observed at  $10.59^\circ$ . The reason for a decline in intensity of the spectra is the addition of external metal ion into the pure  $g\text{-C}_3\text{N}_4$  matrix. The calculated average grain size of Co- $g\text{-C}_3\text{N}_4$ , Ni- $g\text{-C}_3\text{N}_4$ , Fe- $g\text{-C}_3\text{N}_4$  catalysts are 4.3, 4.8, and 5.7 nm respectively. The negligible difference in spectral calibration between pure  $g\text{-C}_3\text{N}_4$  and metal doped  $g\text{-C}_3\text{N}_4$  is due to the doping of trace amount of transition metal ions. Further the XRD result indicates that the sample is free from other kinds of impurities such as initial and intermediate products. Brunauer–Emmett–Teller (BET) analysis was carried out to explore the specific surface area of a material. Figure 1b represents BET surface area of plot of Co- $g\text{-C}_3\text{N}_4$  sample. The calculated surface area is  $817 \text{ m}^2/\text{g}$ .

To understand the surface morphology of pure  $g\text{-C}_3\text{N}_4$  and metal doped  $g\text{-C}_3\text{N}_4$ , SEM analysis was carried out. Figure 2a–d depicts the SEM micrograph of pure  $g\text{-C}_3\text{N}_4$  and metal doped  $g\text{-C}_3\text{N}_4$  samples. As shown in figure, all the samples exhibit flakes morphology at lower magnification due to the presence of the nanosheet of  $g\text{-C}_3\text{N}_4$  [33]. To determine the composition of the catalyst after doping, EDAX measurements were recorded for the pure and metal

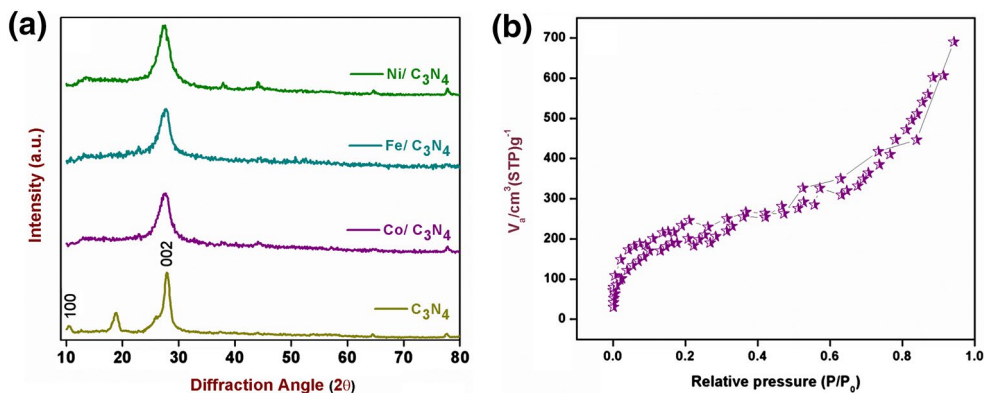


**Fig. 1** a X-ray diffraction patterns of  $g\text{-C}_3\text{N}_4$ , Co- $g\text{-C}_3\text{N}_4$ , Fe- $g\text{-C}_3\text{N}_4$  and Ni- $g\text{-C}_3\text{N}_4$  nanostructure. b BET analysis for Co- $g\text{-C}_3\text{N}_4$

**Fig. 2** Scanning electron microscopy images of **a** g-C<sub>3</sub>N<sub>4</sub>, **b** Co-g-C<sub>3</sub>N<sub>4</sub>, **c** Fe-g-C<sub>3</sub>N<sub>4</sub> and **d** Ni-g-C<sub>3</sub>N<sub>4</sub> nanostructure

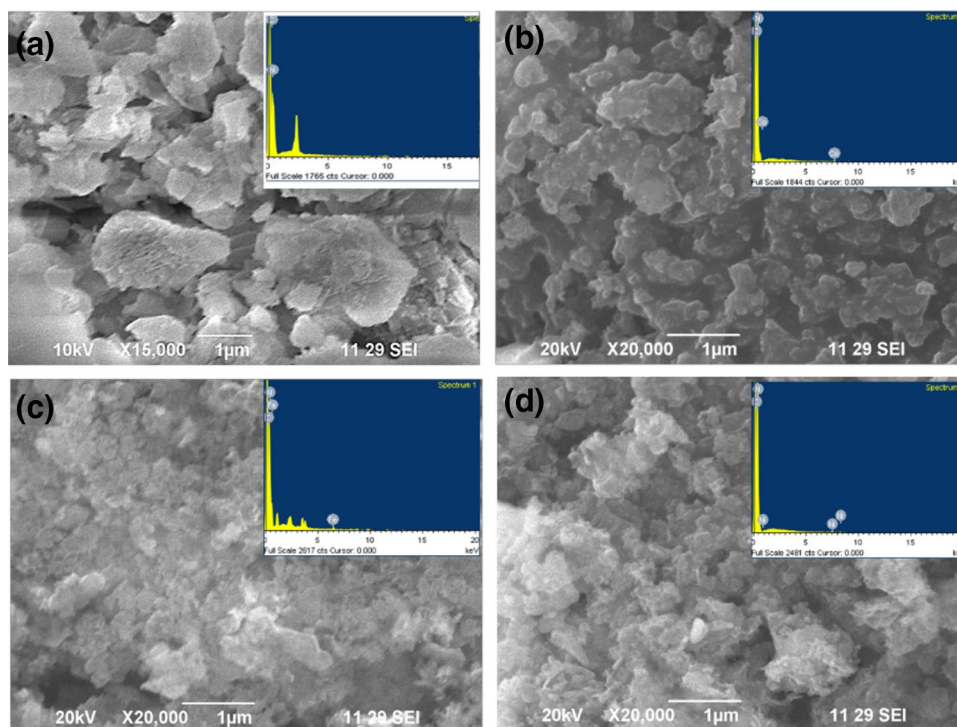


**Table 1** Individual elements of wt% of Co-C<sub>3</sub>N<sub>4</sub>, Ni-C<sub>3</sub>N<sub>4</sub>, and Fe-C<sub>3</sub>N<sub>4</sub>

Sample	C	N	Metal
Pure g-C <sub>3</sub> N <sub>4</sub>	56.23	43.77	–
Ni/g-C <sub>3</sub> N <sub>4</sub>	49.73	50.23	0.03
Fe/g-C <sub>3</sub> N <sub>4</sub>	60.38	39.57	0.05
Co/g-C <sub>3</sub> N <sub>4</sub>	84.36	15.6	0.04

doped samples. Inset Fig. 2a–d illustrates the EDAX spectrum of g-C<sub>3</sub>N<sub>4</sub>, Co-C<sub>3</sub>N<sub>4</sub>, Ni-C<sub>3</sub>N<sub>4</sub>, and Fe-C<sub>3</sub>N<sub>4</sub>. Based on the spectra findings on the pure g-C<sub>3</sub>N<sub>4</sub> and metal doped g-C<sub>3</sub>N<sub>4</sub>, it is evident that only Carbon (C) and Nitrogen (N) are present in addition to the metal ions found in metal doped g-C<sub>3</sub>N<sub>4</sub> (Co, Ni, Fe). The detailed wt% of the individual elements at tabulated in Table 1. There were no additional impurities observed in EDAX, which confirms the successful formation of Co-C<sub>3</sub>N<sub>4</sub>, Ni-C<sub>3</sub>N<sub>4</sub>, and Fe-C<sub>3</sub>N<sub>4</sub>.

The Diffuse reflectance spectroscopy spectra of g-C<sub>3</sub>N<sub>4</sub> and the metal doped g-C<sub>3</sub>N<sub>4</sub> are shown in Fig. 3a. Absorbance maxima of pure g-C<sub>3</sub>N<sub>4</sub> lies at 460 nm, whereas the metal doped samples such as Co-C<sub>3</sub>N<sub>4</sub>, Ni-C<sub>3</sub>N<sub>4</sub>, and Fe-C<sub>3</sub>N<sub>4</sub> exhibit a lower wavelength absorbance maxima. Tauc model was used to calculate the band-gap energy ( $E_g$ ) of the samples which is shown in Fig. 3b. The calculated band gaps for pure g-C<sub>3</sub>N<sub>4</sub>, Co-C<sub>3</sub>N<sub>4</sub>, Ni-C<sub>3</sub>N<sub>4</sub>, and Fe-C<sub>3</sub>N<sub>4</sub> are 2.92, 2.90, 2.86 and 2.85 eV respectively. The lower band gap in the metal doped g-C<sub>3</sub>N<sub>4</sub> is due to the

presence of transition metal ions which enhances absorption of visible light [34].

The analysis of the functional groups present in the catalyst was carried out using the FT-IR spectroscopy technique and is shown in Fig. 4a. In figure, pure g-C<sub>3</sub>N<sub>4</sub> exhibit a broad band at 3186 cm<sup>-1</sup> which can be assigned to the N–H stretching mode. The peak observed at 1634 cm<sup>-1</sup> can be attributed to the presence of C=N stretching vibration frequency. The peaks at 1250 and 1573 cm<sup>-1</sup> can be assigned to the stretching and bending frequency of N–H bond respectively. The lower region peaks observed at 812 and 889 cm<sup>-1</sup> are due to breathing and deformation mode of N–H bond respectively [35]. Other peaks at 1326 and 1417 cm<sup>-1</sup> can be attributed to the presence of aromatic C–N stretching frequencies. On the addition of transition metals, some structural changes are shown in the g-C<sub>3</sub>N<sub>4</sub> functional groups. The stretching and bending frequencies of the metal doped g-C<sub>3</sub>N<sub>4</sub> is slightly different from the pure g-C<sub>3</sub>N<sub>4</sub> matrix. The main characteristic peak of the C=N and C–N stretching vibration frequency of the metal doped g-C<sub>3</sub>N<sub>4</sub> was higher than the pure g-C<sub>3</sub>N<sub>4</sub>. The wavenumber shift was tabulated in Table 2. The shifting of the C=N and C–N stretching frequencies are due to co-ordination a nature of metal ions with the nitrogen atom in the g-C<sub>3</sub>N<sub>4</sub>. The comprehensive results of XRD, SEM-EDAX, UV-DRS and FT-IR measurements confirmed the successful formation of pure g-C<sub>3</sub>N<sub>4</sub>, Co-C<sub>3</sub>N<sub>4</sub>, Ni-C<sub>3</sub>N<sub>4</sub>, and Fe-C<sub>3</sub>N<sub>4</sub>.

Photoluminescence spectra of the catalyst were studied to understand the material defect and the electron hole

**Fig. 3** **a** DRS-UV spectroscopy **b** Tauc plot **c** Fourier transform inferred spectroscopy and **d** Photoluminescence spectra of g-C<sub>3</sub>N<sub>4</sub>, Co-g-C<sub>3</sub>N<sub>4</sub>, Fe-g-C<sub>3</sub>N<sub>4</sub> and Ni-g-C<sub>3</sub>N<sub>4</sub> nano-structure

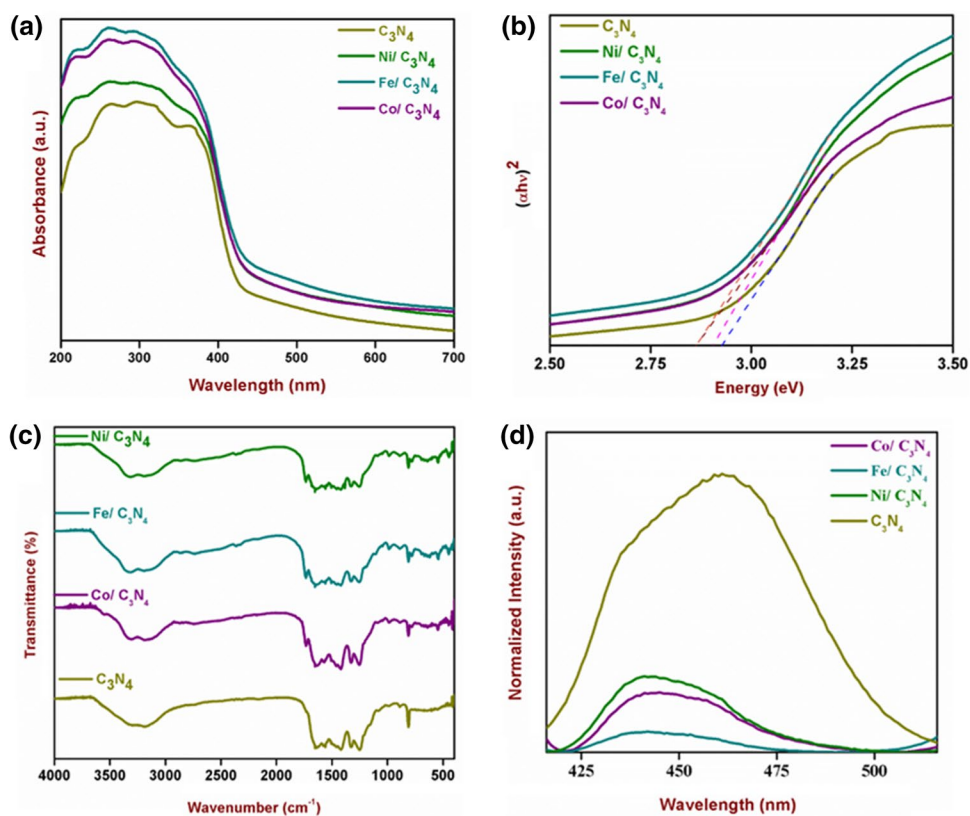


**Fig. 4** PMS-Catalyst, PMS-catalyst-light system degradation of RR120 by **a** Co-g-C<sub>3</sub>N<sub>4</sub>, **b** Fe-g-C<sub>3</sub>N<sub>4</sub> and **c** Ni-g-C<sub>3</sub>N<sub>4</sub> nanostructure and **d** Degradation percentage of RR120 by Co-g-C<sub>3</sub>N<sub>4</sub>, Fe-g-C<sub>3</sub>N<sub>4</sub> and Ni-g-C<sub>3</sub>N<sub>4</sub> nanostructure

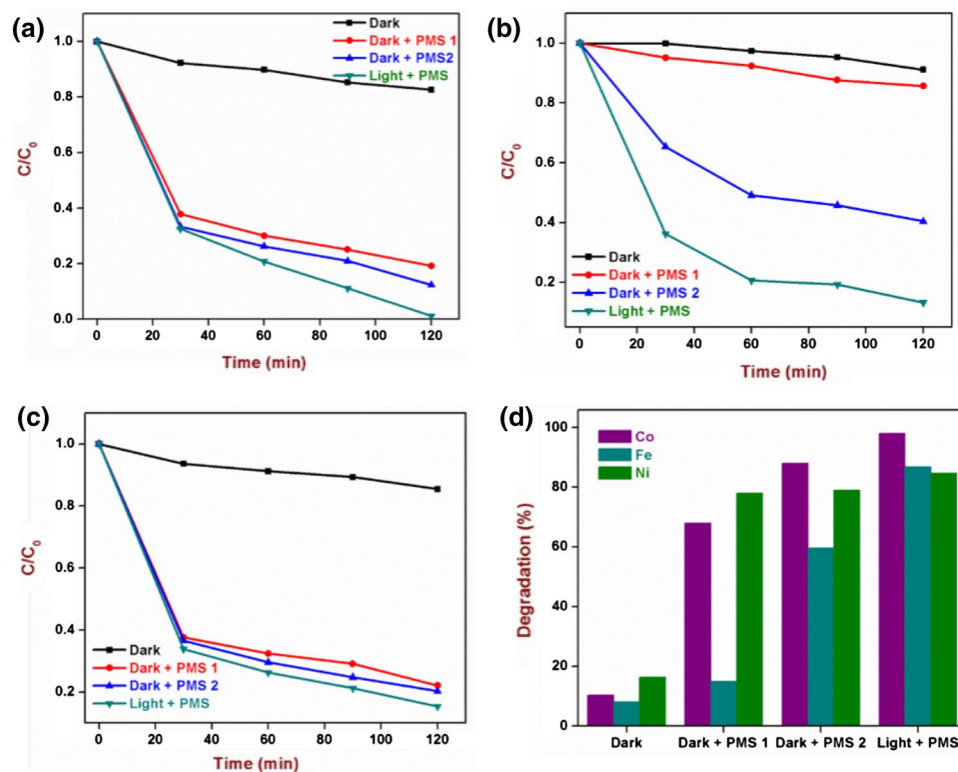


**Table 2** FT-IR Shift for Co-C<sub>3</sub>N<sub>4</sub>, Ni-C<sub>3</sub>N<sub>4</sub>, and Fe-C<sub>3</sub>N<sub>4</sub>

Material	-C=N (cm <sup>-1</sup> )	C-N (cm <sup>-1</sup> )
Pure g-C <sub>3</sub> N <sub>4</sub>	1634	1250
Co/g-C <sub>3</sub> N <sub>4</sub>	1636	1252
Fe/g-C <sub>3</sub> N <sub>4</sub>	1637	1253
Ni/g-C <sub>3</sub> N <sub>4</sub>	1637	1255

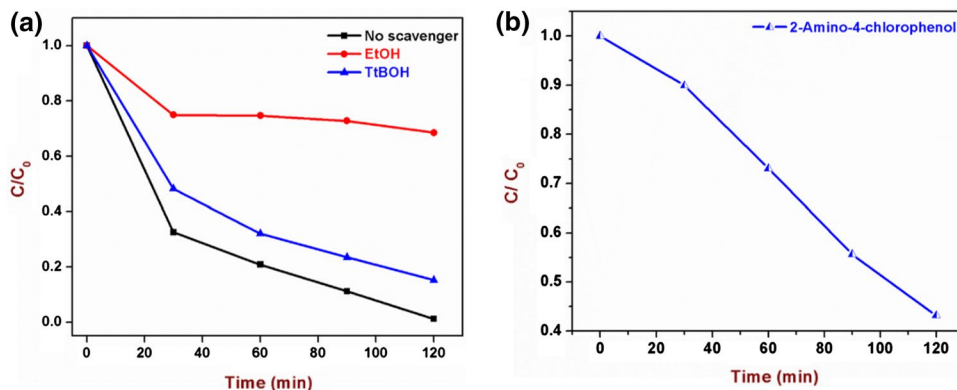
recombination process. The PL spectra is presented in Fig. 4b where the excitation wavelength is observed to be 350 nm [36]. The PL spectra of all samples such as pure g-C<sub>3</sub>N<sub>4</sub>, Co-C<sub>3</sub>N<sub>4</sub>, Ni-C<sub>3</sub>N<sub>4</sub>, and Fe-C<sub>3</sub>N<sub>4</sub> broadly centered between 450 and 460 nm due to the charge recombination. After the metal doping, there is no peak shift which is observed in the PL spectra. However, the intensity of the spectra dramatically decrease in the following order: pure g-C<sub>3</sub>N<sub>4</sub> > Ni-C<sub>3</sub>N<sub>4</sub> > Co-C<sub>3</sub>N<sub>4</sub> > Fe-C<sub>3</sub>N<sub>4</sub>. The reduction in spectral intensity in the metal doped g-C<sub>3</sub>N<sub>4</sub> can be ascribed to the resistance of the metal doped g-C<sub>3</sub>N<sub>4</sub> towards electron hole recombination.

### 3.1 Photocatalytic study and mechanism

After the successful preparation and analysis of the photocatalyst like g-C<sub>3</sub>N<sub>4</sub>, Co-C<sub>3</sub>N<sub>4</sub>, Ni-C<sub>3</sub>N<sub>4</sub>, and Fe-C<sub>3</sub>N<sub>4</sub> its photocatalytic properties were investigated. The photocatalytic efficiency was analyzed for the degradation of various organic pollutants in the absence and in the presence of PMS and visible light. Figure 4a–c represents the relative concentration changes of RR120 degradation by g-C<sub>3</sub>N<sub>4</sub>, Ni-C<sub>3</sub>N<sub>4</sub>, and Fe-C<sub>3</sub>N<sub>4</sub> catalyst with respect to reaction time. Figure 4a shows degradation of RR120 by Co-C<sub>3</sub>N<sub>4</sub> under various experimental conditions such as the catalysts exclusively, PMS + catalyst and PMS-catalyst under visible light condition. The catalyst alone did not degrade the RR120 dye even after 120 min, whereas PMS-Co-C<sub>3</sub>N<sub>4</sub> catalyst exhibit improved degradation under dark conditions. On the other hand, PMS-Co-C<sub>3</sub>N<sub>4</sub>-visible light system possesses a good

catalytic activity for the degradation of RR120 within a time duration of 120 min. In addition, the efficiency of the PMS-Co-C<sub>3</sub>N<sub>4</sub>-visible light system is significantly influenced by the loading of PMS. Likewise other catalyst such as Fe-C<sub>3</sub>N<sub>4</sub> and Ni-C<sub>3</sub>N<sub>4</sub> catalyst was examined under similar conditions and the RR120 degradation is shown in Fig. 4b and c. Figure 4d represents the degradation percentage of RR120 by bare g-C<sub>3</sub>N<sub>4</sub>, Co-C<sub>3</sub>N<sub>4</sub>, Ni-C<sub>3</sub>N<sub>4</sub>, and Fe-C<sub>3</sub>N<sub>4</sub>. All types of catalyst showed below 20% RR120 degradation by catalytic reaction. Ni-C<sub>3</sub>N<sub>4</sub> exhibited 80% of degradation and Fe-C<sub>3</sub>N<sub>4</sub> showed 70% of RR120 degradation in the presence of PMS + catalyst under dark condition. Nearly 100% of RR120 was decomposed by Co-C<sub>3</sub>N<sub>4</sub>-PMS-light system in a duration of 120 min which was the highest degradation observed. There are several types of has been formed during the catalytic reaction such as OH, O<sub>2</sub> and SO<sub>4</sub><sup>-2</sup>. To study the influence of free radicals activity in Co-C<sub>3</sub>N<sub>4</sub>-PMS-light system, radical quenching testes were carried out at the same experimental condition with various scavengers and at different concentrations. The degradation of the dye concentration with respect to time is shown in Fig. 5a. Addition of t-BuOH as a scavenger, did not show any decline in the degradation effects. On the other hand, including EtOH as a scavenger the degradation was observed to decrease rapidly. From this observation it is concluded that SO<sub>4</sub><sup>-2</sup> radical highly influenced the degradation of RR120 when Co-C<sub>3</sub>N<sub>4</sub>-PMS-light system is employed. As a new catalyst, the efficiency should be checked with more than single pollutants. In addition the degradation investigation was carried out on other organic pollutants with dissimilar structure such as phenol derivative like (2-Amino-4-chlorophenol) and orange G using Co-C<sub>3</sub>N<sub>4</sub>-PMS-light conditions. Figure 5b represents the 2-Amino-4-chlorophenol photo degradation in the presence of Co-C<sub>3</sub>N<sub>4</sub>-PMS-light system. At the end of 120 min, the degradation of 2-Amino-4-chlorophenol was nearly 60%. On the other hand Orange G dye entirely degraded in 120 min in the presence of Co-C<sub>3</sub>N<sub>4</sub>-PMS-light system. The degradation UV absorbance spectra are shown in the supporting information (Fig S1). Further the

**Fig. 5** a Effect different radical scavengers on the RR120 degradation b Degradation 2-amino-4-chlorophenol by Co-g-C<sub>3</sub>N<sub>4</sub>-visible light



catalytic activity was analyzed under UV light conditions (i.e.) the RR120 degradation was performed under UV light by Co-C<sub>3</sub>N<sub>4</sub> alone which is shown in Fig. S1(b). The degradation was very poor in UV light when compared to the degradation with visible light in the presence of Co-C<sub>3</sub>N<sub>4</sub>.

### 3.2 Mechanism of the reaction

g-C<sub>3</sub>N<sub>4</sub> is one of the visible light band gap polymeric semiconductor material. When g-C<sub>3</sub>N<sub>4</sub> is exposed to visible light irradiation, the lone bonded valance band electrons move to the conduction band and at the same time equal number of holes are formed in the valance band. Photo induced charge carriers (electron and hole) react with water molecule and surface oxygen results in free radical production (O<sub>2</sub> and OH) [37]. Strong free radical reacts with target molecules to destroy into small and harmless molecules (H<sub>2</sub>O and CO<sub>2</sub>). Very importantly during this process some of the photo induced electron and hole recombined to return to the primary state. To overcome this problem the metal was doped into the original g-C<sub>3</sub>N<sub>4</sub> structure and this dopant reduces the recombination of charge carrier and enhances the light absorbance which has been evidently seen in the PL analysis. Due to this behavior metal doped C<sub>3</sub>N<sub>4</sub> namely Co-C<sub>3</sub>N<sub>4</sub>, Ni-C<sub>3</sub>N<sub>4</sub>, and Fe-C<sub>3</sub>N<sub>4</sub> outperformed when compared to the bare g-C<sub>3</sub>N<sub>4</sub>. On the other hand addition of tiny amount of PMS strongly improved the catalyst efficiency. In the absence of PMS, hydroxyl and superoxide radicals were formed in the photocatalytic reaction. On the contrary, presence of PMS results in sulfate radicals production by the photocatalytic reactions [38]. Indeed, sulfate radicals have much potential in comparison with hydroxyl radicals under the same conditions. Due to their high potential to they quickly degraded the target molecule [39]. Increasing the PMS concentration, resulted in the enhanced degradation efficiency. The calculated pseudo first order rate constant of Co-C<sub>3</sub>N<sub>4</sub> was nearly four times higher than that of Ni-C<sub>3</sub>N<sub>4</sub> and two fold higher than that of Fe-C<sub>3</sub>N<sub>4</sub>. The entire photocatalytic reactions pathways in Fig. 6 are given in the schematic mechanism given as per the observations of the free radical test. The free radical test confirmed that, SO<sub>4</sub><sup>2-</sup> highly influenced the degradation. In addition catalytic reusability test was performed for four cycles on the degradation of RR120 by Co-C<sub>3</sub>N<sub>4</sub>-PMS-visible light. As seen from Fig. 7a, even after four cycles the catalyst maintains

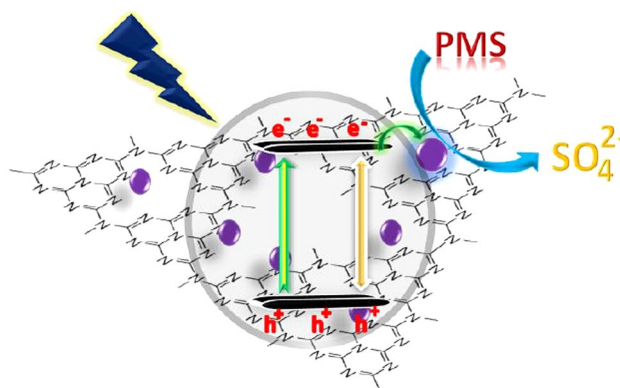


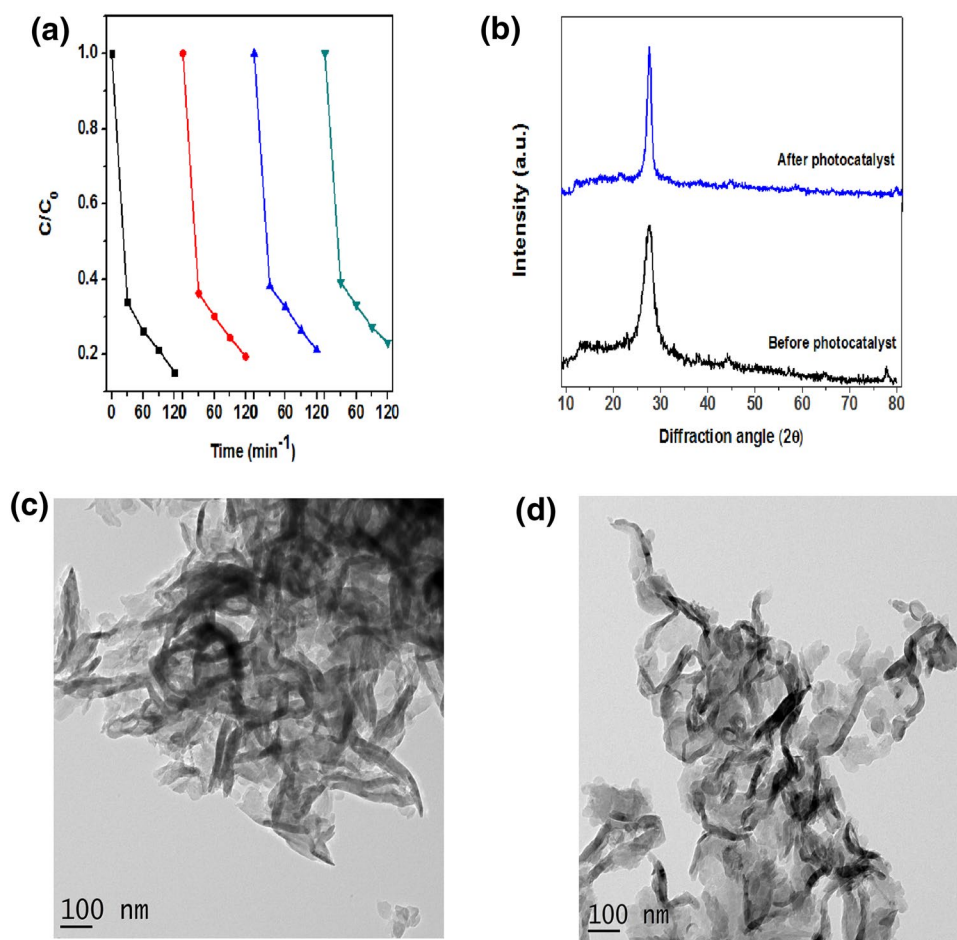
**Fig. 6** Schematic illustration of RR120 degradation by Co-g-C<sub>3</sub>N<sub>4</sub>-visible light system

the same efficiency which ensures reusability of the catalyst. Moreover, to examine the catalyst structural changes after the repeated cycle, XRD and TEM analysis were carried out and compared. Figure 7b represents the XRD spectra of fresh and used Co-g-C<sub>3</sub>N<sub>4</sub> catalyst. No peak shift was observed. Likewise, TEM images are shown in Fig. 7c and d and the sheet like structure is absolutely stable even after the multiple catalyst reactions. From these structural analysis stability of the catalyst is maintained throughout the photocatalytic reaction.

## 4 Conclusion

In conclusion g-C<sub>3</sub>N<sub>4</sub> catalysts were prepared from the pyrolysis of urea and metal doped catalysts were prepared by the sonochemical techniques. Among the prepared catalyst Co-C<sub>3</sub>N<sub>4</sub> exhibits the highest degradation efficiency for RR120, orange G and 2-Amino-4-chlorophenol via PMS activation. The reaction was performed under various experimental conditions to explore the catalytic behavior of the catalyst. The Co-C<sub>3</sub>N<sub>4</sub>-PMS-light showed the reaction rate constant as high as 0.1744 min<sup>-1</sup>, which were 4.3 and 2.1 fold of that of Ni and Fe doped carbon nitride respectively. Enhanced catalytic efficiency could be ascribed to the band gap reduction, decrement of charge carrier recombination and the PMS activation.

**Fig. 7** **a** Catalytic recycle runs for the photocatalytic degradation of RR120 on Co-g-C<sub>3</sub>N<sub>4</sub>-PMS-visible light system **b** XRD for before photocatalyst and after photocatalyst **c** TEM image for Co-g-C<sub>3</sub>N<sub>4</sub> before photocatalytic degradation **d** TEM image for Co-g-C<sub>3</sub>N<sub>4</sub> after photocatalytic degradation



**Acknowledgements** The authors are grateful for the Management and the authorities of Karunya University, Coimbatore, for valuable support and constant encouragement. The authors are grateful to Department of Science and Technology, Govt of India for their financial support.

## References

- K.-T. Chung, *J. Environ. Sci. Heal. Part C*, **34**, 233 (2016)
- Y. Ji, M. Yang, H. Dong, T. Hou, L. Wang, Y. Li, *Nanoscale*, **9**, 8608 (2017)
- N. Li, T. Lv, Y. Yao, H. Li, K. Liu, T. Chen, *J. Mater. Chem. A*, **5**, 3267 (2017)
- Y. Absalan, I.G. Bratchikova, N.N. Lobanov, O.V. Kovalchukova, *J. Mater. Sci. Mater. Electron.* **28**, 18207–18219 (2017)
- L. Wang, Y. Li, S. Li, Y. Wang, W. Kong, W. Xue, C. Li, *J. Mater. Sci. Mater. Electron.* **28**, 17570 (2017)
- A. Mardiroosi, A.R. Mahjoub, H. Fakhri, *J. Mater. Sci. Mater. Electron.* **28**, 11722 (2017)
- S. Thangavel, K. Krishnamoorthy, V. Krishnaswamy, N. Raju, S.J. Kim, G. Venugopal, *J. Phys. Chem. C*, **119**, 22057 (2015)
- M. Rahimi-Nasrabadi, F. Ahmadi, A. Fosooni, *J. Mater. Sci. Mater. Electron.* **28**, 537 (2017)
- M. Rahimi-Nasrabadi, *J. Mater. Sci. Mater. Electron.* **28**, 2200 (2017)
- P. Sun, R. Xue, W. Zhang, I. Zada, Q. Liu, J. Gu, H. Su, Z. Zhang, J. Zhang, and D. Zhang *Catal. Today*, **274**, 2 (2016)
- M.T. Hasan, B.J. Senger, C. Ryan, M. Culp, R. Gonzalez-Rodriguez, J.L. Coffey, and A. V. Naumov, *Sci. Rep.* **7**, 6411 (2017)
- X. Jia, R. Dai, Y. Sun, H. Song, X. Wu, *J. Mater. Sci. Mater. Electron.* **27**, 3791 (2016)
- Y. Cao, Q. Li, W. Wang, *RSC Adv.* **7**, 6131 (2017)
- H.-B. Fang, Y. Luo, Y.-Z. Zheng, W. Ma, X. Tao, *Ind. Eng. Chem. Res.* **55**, 4506 (2016)
- X. Han, L. Tian, H. Jiang, L. Kong, J. Lv, J. Shan, J. Wang, X. Fan, *RSC Adv.* **7**, 14372 (2017)
- L. Shi, L. Liang, F. Wang, M. Liu, K. Chen, K. Sun, N. Zhang, J. Sun, *ACS Sustain. Chem. Eng.* **3**, 3412 (2015)
- M. Shao, Y. Shao, J. Chai, Y. Qu, M. Yang, Z. Wang, M. Yang, W.F. Ip, C.T. Kwok, X. Shi, Z. Lu, S. Wang, X. Wang, H. Pan, *J. Mater. Chem. A*, **5**, 16748 (2017)
- X. Wang, M. Hong, F. Zhang, Z. Zhuang, Y. Yu, *ACS Sustain. Chem. Eng.* **4**, 4055 (2016)
- M. Khairy, W. Zakaria, *Egypt. J. Pet.* **23**, 419 (2014)
- Y.-Y. Ahn, E.-T. Yun, J.-W. Seo, C. Lee, S.H. Kim, J.-H. Kim, J. Lee, *Environ. Sci. Technol.* **50**, 10187 (2016)
- X. Qian, M. Ren, Y. Zhu, D. Yue, Y. Han, J. Jia, Y. Zhao, *Environ. Sci. Technol.* **51**, 3993 (2017)
- H. Huang, H. Lu, H. Huang, L. Wang, J. Zhang, D.Y.C. Leung, *Front. Environ. Sci.* **4**, 17 (2016)
- Y. Yang, J. Jiang, X. Lu, J. Ma, Y. Liu, *Environ. Sci. Technol.* **49**, 7330 (2015)



24. P. Liang, C. Zhang, X. Duan, H. Sun, S. Liu, M.O. Tade, S. Wang, *ACS Sustain. Chem. Eng.* **5**, 2693 (2017)
25. M. Ahmad, A.L. Teel, R.J. Watts, *Environ. Sci. Technol.* **47**, 5864 (2013)
26. S. Verma, S. Nakamura, M. Sillanpää, *Chem. Eng. J.* **284**, 122 (2016)
27. H. Sun, S. Liu, G. Zhou, H.M. Ang, M.O. Tade, S. Wang, *ACS Appl. Mater. Interfaces.* **4**, 5466 (2012)
28. Y. Zhu, S. Chen, X. Quan, Y. Zhang, *RSC Adv.* **3**, 520 (2013)
29. S. Thangavel, N. Raghavan, G. Kadakarai, S.J. Kim, G. Venugopal, *Ultrason. Sonochem.* **24**, 123 (2015)
30. F. Ahmadi, M. Rahimi-Nasrabadi, A. Fosooni, M. Daneshmand, *J. Mater. Sci. Mater. Electron.* **27**, 9514 (2016)
31. M. Rahimi-Nasrabadi, S.M. Pourmortazavi, M.R. Ganjali, P. Norouzi, F. Faridbod, M.S. Karimi, *J. Mater. Sci. Mater. Electron.* **27**, 12860 (2016)
32. F. Fina, S.K. Callear, G.M. Carins, J.T.S. Irvine, *Chem. Mater.* **27**, 2612 (2015)
33. Y. Bu, Z. Chen, T. Xie, W. Li, J.-P. Ao, *RSC Adv.* **6**, 47813 (2016)
34. G. Dong, Z. Ai, L. Zhang, *RSC Adv.* **4**, 5553 (2014)
35. D. Jiang, L. Chen, J. Xie, M. Chen, *Dalt. Trans.* **43**, 4878 (2014)
36. Y. Bao, K. Chen, *Nano-Micro Lett.* **8**, 182 (2016)
37. H. Dong, M. Wei, J. Li, J. Fang, L. Gao, X. Li, A. Xu, *RSC Adv.* **6**, 70747 (2016)
38. H. Shao, X. Zhao, Y. Wang, R. Mao, Y. Wang, M. Qiao, S. Zhao, and Y. Zhu *Appl. Catal. B Environ.* **218**, 810 (2017)
39. Y. Wang, X. Zhao, D. Cao, Y. Wang, Y. Zhu, *Appl. Catal. B Environ.* **211**, 79 (2017)